Chapter 4
Advances in Applied Remote Sensing to Coastal Environments Using Free Satellite Imagery

Cristina Lira and Rui Taborda

Abstract Remote sensing emerges as a very effective technique to capture the dynamics of the coastal system, as it provides a holist view of the system at a wide range of spatial and temporal scales. However, the recent thrive of these systems has led to a broad variety of sensors and data, which can difficult the choice of the optimal sensor for a practical application. In mesoscale coastal environment applications and considering the universe of the solutions, Landsat program arises as a good compromise between spectral, radiometric, spatial and temporal resolutions, combined with free data access, supported by an efficient data sharing platform. The capabilities of the Landsat program was recently extended with the launch of a new satellite – Landsat 8, with improved radiometric and spectral resolution, opening the door to new studies. This work describes the applicability of these images in four case studies that demonstrates the potentialities of the Landsat program in what concerns: (1) time coverage – long-term evolution of an ephemeral ebb delta island; (2) frequency of coverage – seasonal evolution of a short-lived beach; (3) radiometric resolution – shoreline detection and extraction; (4) spectral resolution – bathymetric data retrieval.

4.1 Introduction

The coastal zone is one of the most dynamic areas on Earth, with changes occurring at a wide range of time and spatial scales. This fact, makes systematic mapping of this type of regions a challenge. Thus, the understanding of coastal dynamics

C. Lira (✉)
Instituto Dom Luiz, Centro de Geologia, Geology Department, Faculdade de Ciências da Universidade de Lisboa, Lisbon, Portugal
e-mail: fclira@fc.ul.pt

R. Taborda
Instituto Dom Luiz, Geology Department, Faculdade de Ciências da Universidade de Lisboa, Lisbon, Portugal

C.W. Finkl and C. Makowski (eds.), *Remote Sensing and Modeling: Advances in Coastal and Marine Resources*, Coastal Research Library 9,
DOI 10.1007/978-3-319-06326-3_4,

requires a larger time and spatial scale approach, which time-limited and local studies are incapable of providing. Existing studies, based only on time-limited in situ data collections fall out of date very quickly, due to the constant adjustment to natural forces and human modifications. Therefore, new scientific approaches are needed to improve the understanding of coastal morphology in order to obtain correct evolution models whose application is capable of support management decisions and risk assessment.

From the numerous techniques available to acquire data in coastal systems remote sensing stands out as it can (1) provide a holistic view of the system as the acquired data covers a large area, potentially allowing the observation and understanding of the entire variety of the coastal phenomena; (2) provide data at different temporal scales from hourly to decadal; (3) provide an historical retrospective view of the Earth surface and processes; (4) represents an additional data source, complementing field surveys and in situ measurements.

From the large set of remote sensors currently available, this study focus on the analysis of satellite sensors whose characteristics makes their data suitable to use in mesoscale coastal environment studies, aiming at demonstrating their potentialities and recent advances. This demonstration is supported with several application examples that addresses a range of relevant issues found in several coastal environments. The study targets mesoscale research (i.e. the time scale span months to decades and the spatial scale hundreds of meters to tens of kilometers) since it's increasingly directed towards providing information related to management problems (Horn 2002).

4.2 Remote Sensors: An Overview

From the beginning of remote sensing, about 150 years ago, many different remote sensing systems have been developed to detect and measure energy patterns from different portions of the electromagnetic spectrum (Yang 2009). Nowadays, there is a wide range of remote sensors available and choosing the one that is best for our work can be a challenging task.

Characteristics often used to describe and compare these systems can be grouped into four different types of resolution: spatial, spectral, radiometric, and temporal (Klemas 2011). Spatial requirements include ground resolution (minimum mapping unit) and coverage (swath-width); spectral resolution refers to the number, location and width of the spectral bands; radiometric resolution concerns the pixel depth (i.e. the intensity resolution of each spectral band and the sensor's ability to distinguish between two objects of similar reflectance) and temporal resolution is linked with the frequency of coverage (i.e. hourly, daily, seasonal) and coverage to the extent of the acquisition program (start and end of the period covered for a particular sensor).

With the advent of new technologies, satellites are beginning to overcome the problem of spatial resolutions allowing, simultaneously a good space coverage and a very high ground resolution (<1 m). Additionally, and because there are satellites in space from the 1970s they can also provide a good time-interval coverage.

Table 4.1 Remote sensing constraints in coastal studies

	Open ocean	Estuaries	Beach
Spatial resolution	1–10 km	20–200 m	1–30 m
Coverage area	2,000 × 2,000 km	200 × 200 km	200 × 200 km
Frequency of coverage	1–6 days	0.5 days–decadal	0.5 days–decadal
Radiometric resolution	10–12 bits	8–12 bits	8–12 bits
Spectral resolution	Multispectral/ hyperspectral	Multispetral/ hyperspectral	Multispectral/ hyperspectral

Adapted from Klemas (2009)

Nevertheless, the choice of a specific sensor continues to be a compromise between their main characteristics applied to a specific study, thus the user should familiarize first with the strengths and weaknesses of the available sensors in combination with the desired application. The first step in this process should be the precise identification of the characteristics to extract from the imagery in order to identify the range of sensors that can provide that information. Additionally, sensor choice should depend not only the target spatial, temporal, spectral and radiometric resolutions, but also account for more practical aspects like availability and cost.

Most coastal environments show great variations over larger extents, spatial complexity and temporal variability, which means that these type of environments require high spatial, spectral, radiometric and temporal resolution (Table 4.1, adapted from Klemas 2009). The principle coastal zone related sensors on satellite platforms and their main characteristics and applications are summarized in Table 4.2 (adapted from Klemas 2009, 2011; Mather 2004).

Radar imagery is primarily used in oceanography, imaging the sea surface with the capability to map swell, internal waves, oil slicks, determine sea surface winds and currents, sea level and wave height, etc. (Ikeda and Dobson 1995; Martin 2004), but it lacks the information contained in the visible (VIS) and infra-red (IR) regions of the electromagnetic spectrum. Nevertheless, radar can penetrate fog and clouds, making it valuable in areas where cloud cover persists, particularly, in emergency applications (storms, hurricanes).

The use of very high spatial resolution (VIR) sensors will improve the detail of the analysis, but this kind of image products are available only by commercial companies (high cost) and because they display great detail (ground resolution), they present lower area coverage, lacking the global spatial vision that sometimes coastal studies mandate. Thus, to keep costs practical, large coastal areas should be analyzed using medium to high resolution satellite sensors (15–30 m) and only small and critical areas mapped with airborne or VIR satellite sensors.

4.2.1 The Landsat Program

With over 40 years of collecting spectral information from Earth's surface and creating an historical archive unmatched in quality, detail, coverage, and length,

Table 4.2 Principal coastal zone related sensors and their main characteristics

		Spectral band		SR	RR	Cycle	Swath width			
Satellite	Sensor	Number	(μm)	(m)	bits	(days)	(km)	Temporal coverage	Availability	Applications
Landsat 1, 2, 3	MSS	4 – Green	0.5–0.6	60[a]	8	18	185	1972–1983	F	LULC
		5 – Red	0.6–0.7	60[a]	8	18	185			CD
		6 – NIR	0.7–0.8	60[a]	8	18	185			V
		7 – NIR	0.8–1.1	60[a]	8	18	185			CA
Landsat 4, 5	TM	1 – Blue	0.45–0.52	30	8	16	185	1982–2012	F	
		2 – Green	0.52–0.60	30	8	16	185			
		3 – Red	0.63–0.69	30	8	16	185			
		4 – NIR	0.76–0.90	30	8	16	185			
		5 – NIR	1.55–1.75	30	8	16	185			
		6 – Thermal IR	10.40–1.50	30	8	16	185			
		7 – MIR	2.08–2.35	120	8	16	185			
Landsat 7	ETM+	1 – Blue	0.45–0.52	30	8	16	185	1999 – now	F	
		2 – Green	0.52–0.60	30	8	16	185			
		3 – Red	0.63–0.69	30	8	16	185			
		4 – NIR	0.77–0.90	30	8	16	185			
		5 – NIR	1.55–1.75	30	8	16	185			
		6 – Thermal IR	10.40–12.50	60	8	16	185			
		7 – MIR	2.08–2.35	30	8	16	185			
		8 – PAN	0.52–0.90	15	8	16	185			
Landsat 8	OLI	1 – Coastal aerosol	0.43–0.45	30	16	16	185	2013 – now	F	
		2 – Blue	0.45–0.51	30	16	16	185			
		3 – Green	0.53–0.59	30	16	16	185			
		4 – Red	0.64–0.67	30	16	16	185			
		5 – NIR	0.85–0.88	30	16	16	185			
		6 – SWIR 1	1.57–1.65	30	16	16	185			

		7 – SWIR 2	2.11–2.29	30	16	16	185			
		8 – PAN	0.50–0.68	15	16	16	185			
		9 – Cirrus	1.36–1.38	30	16	16	185			
	TIRS	10-Thermal IR	10.60–11.19	100[b]	16	16	185			
		11-Thermal IR	11.50–12.51	100[b]	16	16	185			
SPOT 1, 2, 3	HVR	1 – Green	0.50–0.59	20	8	26	60	1986–2009	C/A	LULC
		2 – Red	0.61–0.68	20	8	26	60			CD, CA
		3 – NIR	0.79–0.89	20	8	26	60			
		PAN	0.50–0.73	10	8	26	60			
SPOT 4	HRVIR	B1 – Green	0.50–0.59	20	8	5	60	1998 – now	C	LULC
	VGT	B2 – Red	0.61–0.68	20	8	5	60			CD, CA
		B3 – NIR	0.78–0.89	20	8	5	60			V, DEM
		B4 – SWIR	1.58–1.75	20	8	5	60			B
		PAN	0.61–0.68	10	8	5	60			
SPOT 5	HRG	PAN	0.48–0.71	2.5–5	8	2–3	60	2002 – now	C	LULC
		B1 – Green	0.50–0.59	10	8	2–3	60			CD, CA
		B2 – Red	0.61–0.68	10	8	2–3	60			V, DEM
		B3 – NIR	0.78–0.89	10	8	2–3	60			B
		B4 – SWIR	1.58–1.75	20	8	2–3	60			
IKONOS		1 – Blue	0.45–0.52	3.2	11	<3	11.3	1999 – now	C	CA, B
		2 – Green	0.52–0.60	3.2	11	<3				V, DEM
		3 – Red	0.63–0.69	3.2	11	<3				
		4 – NIR	0.76–0.90	3.2	11	<3				
		5 – PAN	0.45–0.90	0.82	11	<3				
NOAA	AVHRR	1 – Red	0.58–0.68	1,100	10	2/day	2,400	1978 – now		V, Cir
	LAC	2 – NIR	0.725–1.1	1,100	10	2/day	2,400			
		3 – SWIR	3.55–3.93	1,100	10	2/day	2,400			
		4 – MIR	10.5–11.3	1,100	10	2/day	2,400			
		5 – Thermal IR	11.5–12.5	1,100	10	2/day	2,400			

(continued)

Table 4.2 (continued)

		Spectral band		SR	RR	Cycle	Swath width			
Satellite	Sensor	Number	(μm)	(m)	bits	(days)	(km)	Temporal coverage	Availability	Applications
Orbview 2	SeaWiFS	1 – Violet	404–422	1,100	10	1	2,800	1997 – now	C/F	OC
		2 – Blue	433–453	1,100	10	1	2,800			
		3 – Blue-Green	480–500	1,100	10	1	2,800			
		4 – Blue-Green	500–520	1,100	10	1	2,800			
		5 – Green	545–565	1,100	10	1	2,800			
		6 – Red	660–680	1,100	10	1	2,800			
		7 – NIR	745–785	1,100	10	1	2,800			
		8 – NIR	845–885	1,100	10	1	2,800			
QuicBird		1 – Blue	450–520	2.44	11	1–3.5	16.5	2001 – now	C	LULC
		2 – Green	520–60	2.44	11	1–3.5	16.5			CD, CA
		3 – Red	630–690	2.44	11	1–3.5	16.5			V, B
		4 – NIR	760–890	2.44	11	1–3.5	16.5			
		5 – PAN	450–900	0.61	11	1–3.5	16.5			
GeoEye		1 – Blue	450–510	1.65	11	2.1–8.3	15.2	2008 – now	C	LULC
		2 – Green	510–580	1.65	11	2.1–8.3	15.2			CD, CA
		3 – Red	655–690	1.65	11	2.1–8.3	15.2			V, B
		4 – NIR	780–920	1.65	11	2.1–8.3	15.2			
		5 – PAN	450–800	0.41	11	2.1–8.3	15.2			
WorldView 2		1 – Coastal Blue	400–450	2	11	1.1–2.7	16.4	2008 – now	C	LULC
		2 – Blue	450–510	2	11	1.1–2.7	16.4			CD, CA
		3 – Green	510–580	2	11	1.1–2.7	16.4			V, B, DEM
		4 – Yellow	585–625	2	11	1.1–2.7	16.4			
		5 – Red	630–690	2	11	1.1–2.7	16.4			

		6 – NIR	705–745	2	11	1.1–2.7	16.4			
		7 – NIR	770–1,040	2	11	1.1–2.7	16.4			
		8 – PAN	450–800	0.5	11	1.1–2.7	16.4			
ASTER	VNIR	1 – Green	0.52–0.60	15	8	16	60	1999 – now	F[c]	LULC
		2 – Red	0.63–0.69	15	8	16	60			CD
Terra		3 – NIR	0.76–0.86	15	8	16	60			V
	SWIR	4	1.600–1.700	30	8	16	60			B
		5	2.145–2.185	30	8	16	60			CA
		6	2.185–2.225	30	8	16	60			
		7	2.235–2.285	30	8	16	60			
		8	2.295–2.365	30	8	16	60			
		9	2.360–2.430	30	8	16	60			
	TIR	10	8.125–8.475	90	12	16	60			
		11	8.475–8.825	90	12	16	60			
		12	8.925–9.275	90	12	16	60			
		13	10.25–10.95	90	12	16	60			
		14	10.95–11.65	90	12	16	60			
ASAR	ENVISAT	1	C – band	30		<3	500	2002–2012	C/A	Cir, W
		2	4 pol							
RADARSAT –1, 2	1	C – band	10–100	16	26	100	1995–now	C	MS, I, LULC	

Adapted from Klemas (2009), Klemas (2011), and Mather (2004)

A Available under project submission, *B* Bathymetry, *C* Commercial, *CA* Coastal applications dynamics, *CD* Change detection, *Cir* Circulation, *DEM* Digital elevation models, *F* Available on-line for free download, *I* Ice, *LULC* Land use land cover, *MIR* Middle Infrared, *MS* Marine surveillance, *NIR* Near Infrared, *OC* Ocean Color, *PAN* Panchromatic, *RR* Radiometric resolution, *SR* Spatial Resolution, *SWIR* Shortwave Infrared, *V* Vegetation, *W* Waves

[a]Original MSS pixel size was 79 × 57 m; production systems now resample the data to 60 m

[b]Resampled to 30 m to match multispectral bands

[c]ASTER level-1B data products over the U.S. and Territories from the NASA ASTER mission

Landsat program has offered the world with continuous and consistent monitoring of critically important global resources from which coastal subjects are no exception. Additionally, as of December 2009 all Landsat data in the USGS archive became free[1] to the public, which has, since then, stimulated the use of multispectral imagery in coastal applications.

Besides the fact that Landsat data is freely available online, it is used in coastal studies because it is systematically collected (high temporal frequency), provides large footprints (allowing meso to macro spatial scale studies), has the largest satellite data available historic archive (highest temporal coverage) and provides information on the VIS and IR ranges of the electromagnetic spectrum, where the major coastal information is registered.

Landsat images have been used in different type of studies: in coastal management the National Oceanic and Atmospheric Administration Coastal Change Analysis Program (NOAA) uses Landsat 5 to provide coastal managers with consistent and reliable source of information; shoreline evolution was successfully analyzed from Landsat images (Yu et al. 2011; Ahmad and Lakhan 2012; Huang et al. 2012; Mukhopadhyay 2012); Klemas (2001) uses this imagery to detect coastal environmental indicators; Ryu et al. (2008) derive intertidal morphology and Pe'eri et al. (2012) states that multispectral satellite remote sensing, such as Landsat, is capable of characterize bathymetry information in clear shallow-water.

Nevertheless, Landsat is not free from limitations. The medium spatial resolution can hinder more local studies or extraction of very small characteristics and the use of VIR images can became necessary when studying small objects. Additionally, Landsat images are also dependent upon cloud coverage limiting the use of valuable information on clear sky days or low cloud coverage.

4.3 The Landsat Operational History

Landsat 1 was launched on July 23, 1972 and known, at that time, as the Earth Resources Technology Satellite (ERTS) and operated until January 1978, outliving its design life by 5 years. It was the first Earth-observing satellite to be launched with the express intent to study and monitor our planet's landmasses (NASA). It carried two instruments: a camera system built by the Radio Corporation of America (RCA) called the Return Beam Vidicon (RBV), and the Multispectral Scanner (MSS) (Short et al. 1976).

Landsat 2 was launched on January 22, 1975, and removed from operation on February 25, 1982, due to yam control problems. Still considered an experimental project and operated by NASA, Landsat 2 carried the same sensors as its predecessor: the RBV and the MSS. Landsat 3 was launched on March 5, 1978 and putted on

[1] As of October 1, 2008, all Landsat 7 data became free to the public. In December 2009, all Landsat data in the USGS archive followed suit.

standby mode on March, 1983, being decommissioned on September 7, 1983. Landsat 3 carried the same sensors as its predecessor, but RBV instrument had an improved 38 m ground resolution and used two RCA cameras which both imaged in one broad spectral band (green to near-infrared; 0.505–0.750 μm) instead of three separate bands (green, red, infrared) like its predecessors (Mika 1997; USGS).

Launched on July 16, 1982, Landsat 4 was significantly different than the former and did not carry the RBV instrument. In addition to the MSS instrument, Landsat 4 (and Landsat 5) carried a sensor with improved spectral and spatial resolution, known as the Thematic Mapper (TM). This instrument had seven spectral bands, collecting data from the blue, green, red, near-infrared, mid-infrared (two bands) and thermal infrared portions of the electromagnetic spectrum. Within a year of its launch Landsat 4 experienced problems and the data downlink capability was lost completely in 1993 (USGS).

Carrying the same payload, the MSS and the TM instruments as its predecessor, the Landsat 5 was launched on March 1, 1984, which was designed and built at the same time as Landsat 4. In 1987, its TDRSS transmitter (Ku-band) failed making downlinking data acquired outside the range of U.S. ground receiving antennas impossible. The MSS instrument was turned off in August of 1995 and in November 2011, the TM instrument stopped acquiring images due to a rapidly degrading electronic component. A few months later, engineers turned the MSS instrument back on, and implemented new capabilities to ingest the raw instrument data at the ground station. USGS announced, on December 21, 2012, that Landsat 5 would be decommissioned. Nevertheless, Landsat 5 outlived its 3-year design life, delivering high-quality and global data for 28 years and 10 months, which officially set a new Guinness World Records title for "Longest-operating Earth observation satellite."

During the life span of the Landsat 5, the Landsat program experienced a privatization era, during which Landsat coverage standards declined and many observations from 1984 to 1999 were missed because there was no obvious and immediate buyer (Williamson 1997; Goward and Williams 1997). On July 1, 2001, operational control was officially returned to the federal government, which also relinquished their commercial right to Landsat data.

On April 15, 1999, Landsat 7 was successfully launched carrying the Enhanced Thematic Mapper Plus (ETM+) Earth observing instrument, which replicates the capabilities of the highly successful TM instruments. This new sensor included additional features that make it a more versatile and efficient instrument for global change studies, land cover monitoring and assessment, and large area mapping than its design forebears: a panchromatic band with 15 m spatial resolution, an on-board, full aperture, 5 % absolute radiometric calibration, a thermal IR channel with 60 m spatial resolution and an on-board data recorder (USGS). Landsat 7 experienced a failure of its scan line corrector (SLC) on May 2003, and since then Landsat 7 have been acquiring images with SLC-off mode, but the ETM + still acquires approximately 75 % of the data for any given scene and images continued to be highly used.

4.4 The New Landsat 8

This year, the Landsat program has given us another step forward, with the launch of Landsat 8 sensor, with new functionalities. Landsat 8 was launched on February 11, 2013, with a payload consisted of two science instruments – the Operational Land Imager (OLI) and the Thermal Infrared Sensor (TIRS). These two sensors provide seasonal coverage of the global landmass and surrounding areas at a spatial resolution of 30 m (visible, NIR, SWIR); 100 m (thermal); and 15 m (panchromatic), every 16 days. These new instruments represent an evolutionary advance in technology. OLI is a push-broom sensor with a four-mirror telescope and 12-bit quantization, collects data for visible, near infrared, and short wave infrared spectral bands as well as a panchromatic band. It has a 5-year design lifetime (USGS). The comparison between OLI spectral bands to Landsat 7's ETM + bands can be seen in Table 4.1. OLI provides two new spectral bands, one tailored especially for detecting cirrus clouds and the other for coastal zone observations. TIRS collects data for two more narrow spectral bands in the thermal region formerly covered by one wide spectral band on Landsat 4–7, with a spatial resolution of 100 m and also a 12-bit quantization. Landsat 8 is required to return 400 scenes per day to the USGS data archive (150 more than Landsat 7), increasing the probability of capturing cloud-free scenes for the global landmass, scene size is 185-km-cross-track-by-180-km-along-track and a cartographic accuracy of 12 m or better (including compensation for terrain effects).

4.5 Application Examples

The following application examples, applied in four different sites (Fig. 4.1) intend to address four main characteristics of the Landsat program, highlighting its potentialities in coastal environment uses: (1) time coverage; (2) frequency of coverage; (3) radiometric resolution and (4) spectral resolution. Figure 4.1 displays the location of the four study sites: A – Long-term evolution of the Bugio ephemeral ebb delta island; B – Seasonal evolution of the Prainha transient beach; D – Shoreline detection and extraction along the Costa da Caparica's beaches and D – Bathymetric data retrieval on Sado ebb delta.

4.5.1 Shoreline Detection and Extraction

In the geological context, processes of erosion, transport and deposition involve the removal, transport and deposition of a quantity of material which, from the viewpoint of the shoreline concept implies considering the shore as a three-dimensional surface whose shape is constantly changing. In this context the shoreline is set with

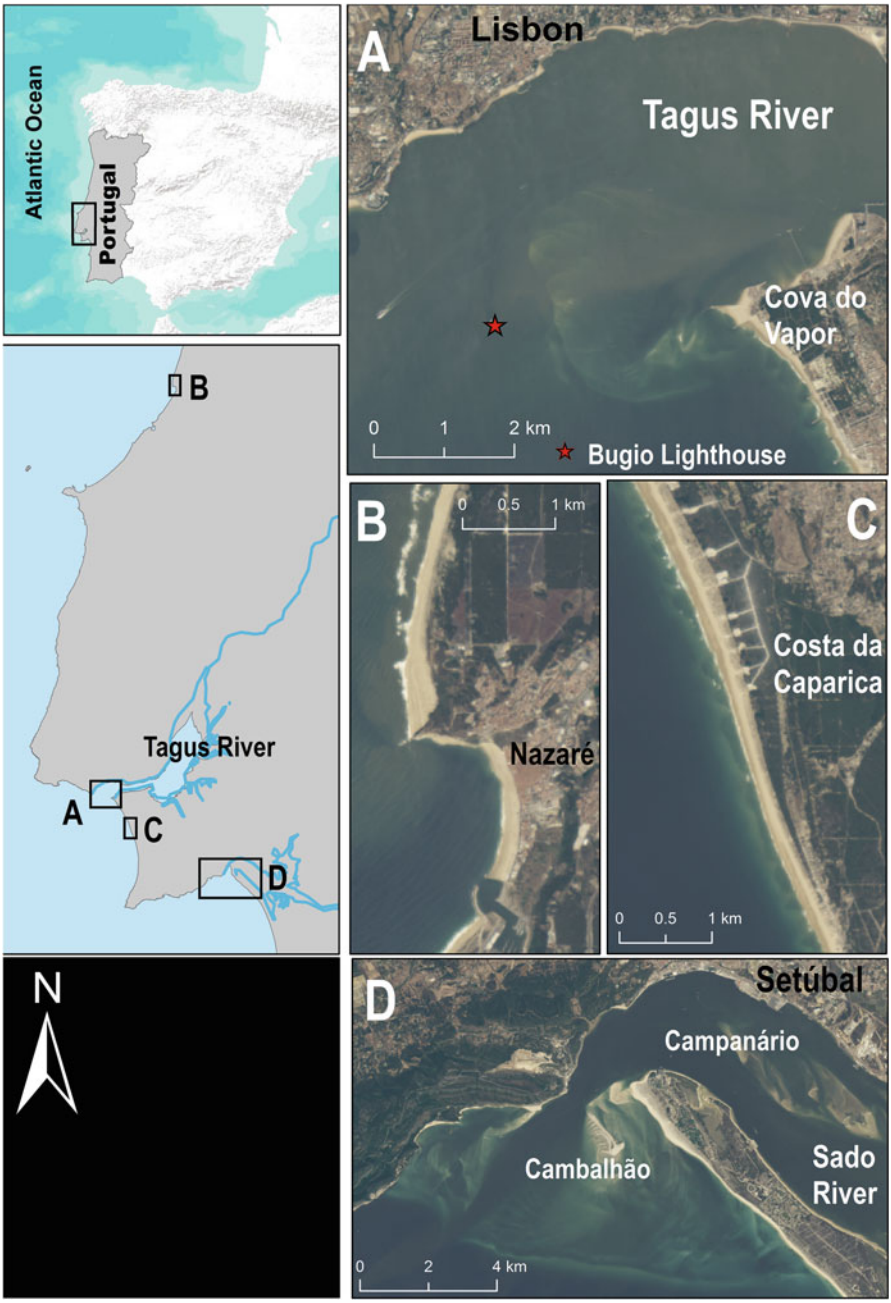

Fig. 4.1 Location of the study sites. (**a**) Long-term evolution of the Bugio ephemeral ebb delta island; (**b**) Seasonal evolution of the Prainha transient beach; (**c**) Shoreline detection and extraction and (**d**) Bathymetric data retrieval on Sado ebb delta. Basemap: 2013-09-08 Landsat 8 image

a principal objective: to characterize the mobility of the sand in space through time. Even considering a static sandy coastline, the shoreline, regarded as the water/land interface, changes because the water level is constantly changing. However, in what concerns context of coastal evolution this concept should necessarily be independent of water level variations. Due to the extremely dynamic nature of the concept, its definition has rely on several criteria. The adopted criteria should be the one that best lists and quantifies the beach horizontal/vertical relations in the sense that it is both robust and reproducible. Boak and Turner (2005) lists a variety of shoreline criteria, which depending of the data source has different capabilities and limitations. According to Parker (2003), the best shoreline definition is the one least susceptible to variability that is not related to actual physical changes in the shoreline itself as, for example, the dune toe. However, in remote sensing applications the HWL (high water level) mark is most commonly adopted criteria as is a feature very simple to identify (sometimes is the only possible) despite the several drawbacks widely acknowledged. For example, Morton and Speed (1998) state this is not a morphological feature, but instead an ephemeral "line in the sand", sensitive to short-term fluctuations in wave and tide conditions. Recent advances in the radiometric resolution of satellite imagery eases the recognition of more robust proxies that depends on differences in the radiometric intensity.

Radiometric resolution is a measure of a sensor's ability to distinguish between two objects of similar reflectance, and higher radiometric resolutions is capable of improving the distinctions between reflectance values. Landsat 8 sensors provide improved signal-to-noise (SNR) radiometric performance quantized over a 12-bit dynamic range, which turns into 4,096 potential grey levels in an image compared with only 256 grey levels in previous versions. Improved signal to noise performance is capable of improving the characterization of land cover, such as shoreline detection using the vegetation line.

This application example try to exploit the improved radiometric resolution of the Landsat images to support the shoreline extraction process. In this case, the shoreline is based on the seaward vegetation line, used as dune toe proxy.

4.5.1.1 Methodology

The shoreline was extracted from two satellite images: a Landsat 5 image dated of 2010-07-30 and a Landsat 8 image of 2013-09-08 along a sandy shoreline stretch (Fig. 4.1c). Detection and extraction was made manually by digitizing the visible vegetation line in ArcGIS 10.1 following Ford (2013). A consistent scale was used and the definition of the vegetation boundary highlighted with the false color composition of 742 bands (Landsat 5) and 753 (Landsat 8), joint with the true color composition. Shoreline results were compared with the shoreline extracted from the 2010 orthophotomaps with 0.5 m of spatial resolution (baseline) of the same area using the same proxy. The two satellite derived shorelines were compared with the baseline using the Digital Shoreline Analysis System (DSAS) (Thieler et al. 2009).

Table 4.3 Mean distance and root mean square error (RMSE) between the two Landsat images and the baseline

Landsat sensor	Date	Mean distance (m)	RMSE (m)
TM	2010-07-30	9.44	12.47
OLI	2013-09-08	5.98	7.27

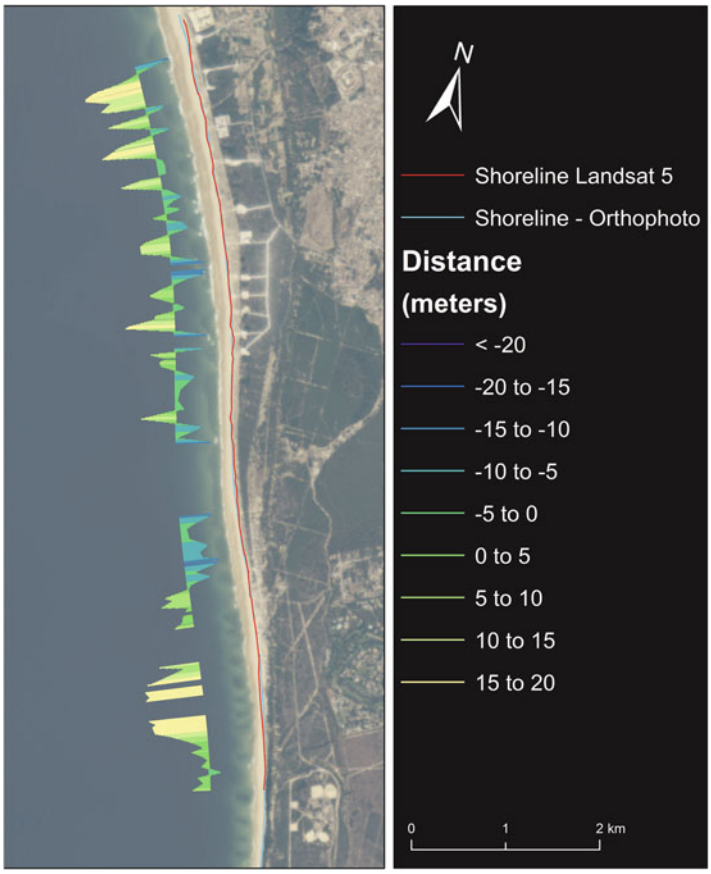

Fig. 4.2 Deviation along the shoreline extracted from the Landsat 5 (2010-07-30)

4.5.1.2 Results

Table 4.3 presents the results of the comparison between lines identified and extracted from satellite imagery and a baseline digitized over a high resolution orthophotomap. The Landsat 5 had a mean distance error of 9.44 m with 12.47 m of RMSE; and Landsat 8 was able to extract the same line with a mean distance error of 5.98 m and 7.27 m of RMSE. Spatial differences alongshore are represented in Figs. 4.2 and 4.3. Results show that Landsat 8 enhanced radiometric resolution can

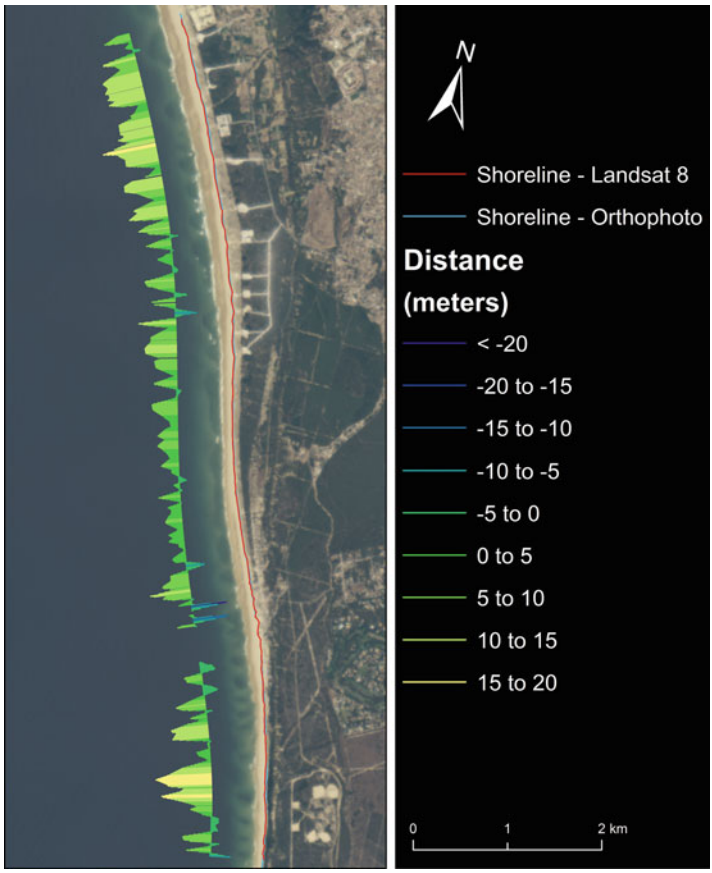

Fig. 4.3 Deviation along the shoreline extracted from the Landsat 8 (2013-09-08)

help to improve the shoreline detection procedure, making it useful in shoreline evolution studies of extremely dynamic and large coastline environments.

4.5.2 Long-Term Evolution of an Ephemeral Ebb Delta Island

River mouths are coastal regions with particularly complex morphodynamic characteristics. Knowledge of the temporal and spatial evolution of these spaces is fundamental to the understanding of their dynamics and to define the sediment budget of the adjacent coastal sectors. A notable element of this dynamic is associated with the development of emerged sand bodies, with extremely variable configuration in space and time that often exhibit an ephemeral nature. Such case is

the Bugio Island, located in the Tagus ebb delta (Fig. 4.1a). The evolution of this island has exhibited a pattern where long (pluri-annual) stabilization periods alternate with sudden changes in its configuration, in a clear link to the adjacent coastal area. The main objective of this application example was to study the evolution of the configuration and location of the emerged section of the Bugio sandbank through the use of satellite images from Landsat program over the past 40 years. The long time coverage of the Landsat program makes it the ideal tool to study the decadal evolution of these dynamic areas, especially in cases where other data sources are not available. This is the case of the Tagus ebb delta where the limited information available makes Landsat images an invaluable asset.

4.5.2.1 Methodology

The outline of Bugio Island was defined by the land-water interface extracted from the different Landsat images using the ratio between two bands: b2/b4, for TM and ETM + images and b1/b4 and b3/b6 for the MSS imagery (Alesheikh et al. 2007; Gens 2010). Results drove to a successful mapping of the shoreline; root mean square error (RMSE), computed from the automatic extraction of the Bugio Lighthouse, was estimated in 20.6 m which corresponds to a subpixel precision for all spatial resolutions used (Table 4.4). This data was complement with an aerial photography dated from 1958.

4.5.2.2 Results

Aerial photographs from 1958 show that the Bugio Island was located ~1 km NE of the Bugio lighthouse and displayed an elongated horseshoe-shape. Results of the analysis of satellite images are summarized in Figs. 4.4, 4.5 and Table 4.4. Between 1973 and 1984 the position of Bugio Island did not change significantly but exhibited relevant changes in shape, which altered from a double islet configuration to a single trapezoidal shape and a u-shape with a bay opened to the estuary. In 1987, Bugio Island enlarges and display an arcuate configuration, with the convex side pointing seaward. Afterwards, the island suffers a counterclockwise rotation and progressively stretched towards Cova do Vapor. From 1993 onwards, the area of the island was progressively reduced until its disappearance in 2002. The results show very irregular evolution and dynamics of Bugio Island, with periods of relative stability alternating with episodes in which the variations are extremely fast (Fig. 4.4). This example shows the potential of using the full temporal range of the Landsat program, allowing to know the past in a striving to understand the future.

Table 4.4 Landsat images used is the study, date, time and respective tide level

Landsat sensor	Date	Time (UTC)	Resolution (m)	Tide (MSL) (m)	Landsat sensor	Date	Time (UTC)	Resolution (m)	Tide (MSL) (m)
MSS	1973-03-29	10:50:40	60	0.44	TM	1992-07-12	10:37:46	30	0.57
MSS	1975-08-01	10:37:53	60	0.41	TM	1993-07-31	10:38:15	30	0.57
MSS	1977-04-21	10:15:00	60	−1.12	TM	1994-07-02	10:33:14	30	0.67
MSS	1978-11-01	10:22:22	60	−0.67	TM	1995-07-21	10:19:18	30	0.79
TM	1984-05-03	10:41:43	30	−0.88	TM	1996-08-08	10:30:24	30	0.86
TM	1987-07-31	10:40:07	30	−0.69	TM	1997-07-26	10:45:35	30	−0.09
TM	1988-12-16	10:46:23	30	0.22	TM	1998-08-30	10:53:00	30	0.12
TM	1989-03-14	10:43:00	30	−0.02	TM	1999-07-08	11:07:17	30	0.71
TM	1990-12-22	10:39:28	30	−0.79	ETM+	2000-11-15	11:04:51	30	−1.22
TM	1991-08-11	10:37:08	30	0.95	ETM+	2001-05-26	11:04:19	30	−1.04

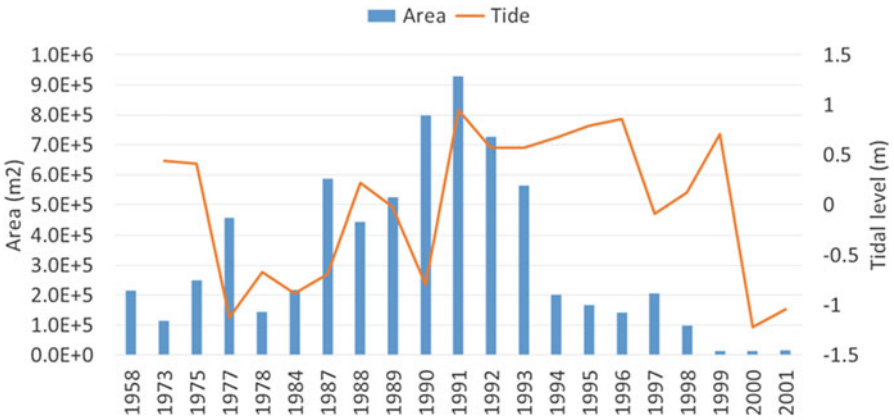

Fig. 4.4 Evolution of the Bugio Island area over the period 1958–2001 and the respectively tidal level of each Landsat image used

4.5.3 Seasonal Evolution of a Transient Beach

Seasonal beach changes can be connected to both cross-shore and longshore sediment transport processes: while the former relates to the transference of sand along the beach profile, reflecting the natural adjustment of the beach profile to the seasonal changes in wave energy, the latter is connected to modifications in planform geometry, usually in relation to seasonal changes in wave direction.

The detection of these changes, depends not only on an adequate temporal coverage but also on the relation between the magnitude of the changes and spatial resolution of the satellite imagery. For the large majority of cases this inhibits the application of this methodology to the evaluation of cross-shore changes. On the other hand, planform changes, usually related with beach rotation or sediment headland bypassing, can attain a magnitude compatible with satellite resolution making this technique suitable for the study of these processes.

The case study used to demonstrate satellite imagery potential to the study of these processes concerns to a transient beach in relation to headland sediment bypassing of Nazaré headland, the Prainha beach (Figs. 4.1b and 4.6). This beach usually grows in summer, in connection to the low energetic, short period, northerly waves, that promotes sediment bypassing and fades out in early autumn with the onset of higher energetic waves.

4.5.3.1 Methodology

The shoreline was extracted using the water/land boundary using the Red (Band4)/ NIR (band5) ratio of the Landsat 8 imagery. Line elevation was estimated from the tide level at the time of acquisition. Results were validated using three fieldwork topographic surveys dated from 2013-09-19, 2013-10-09 to 2013-10-13, more or less concomitant with three satellite images (Fig. 4.7).

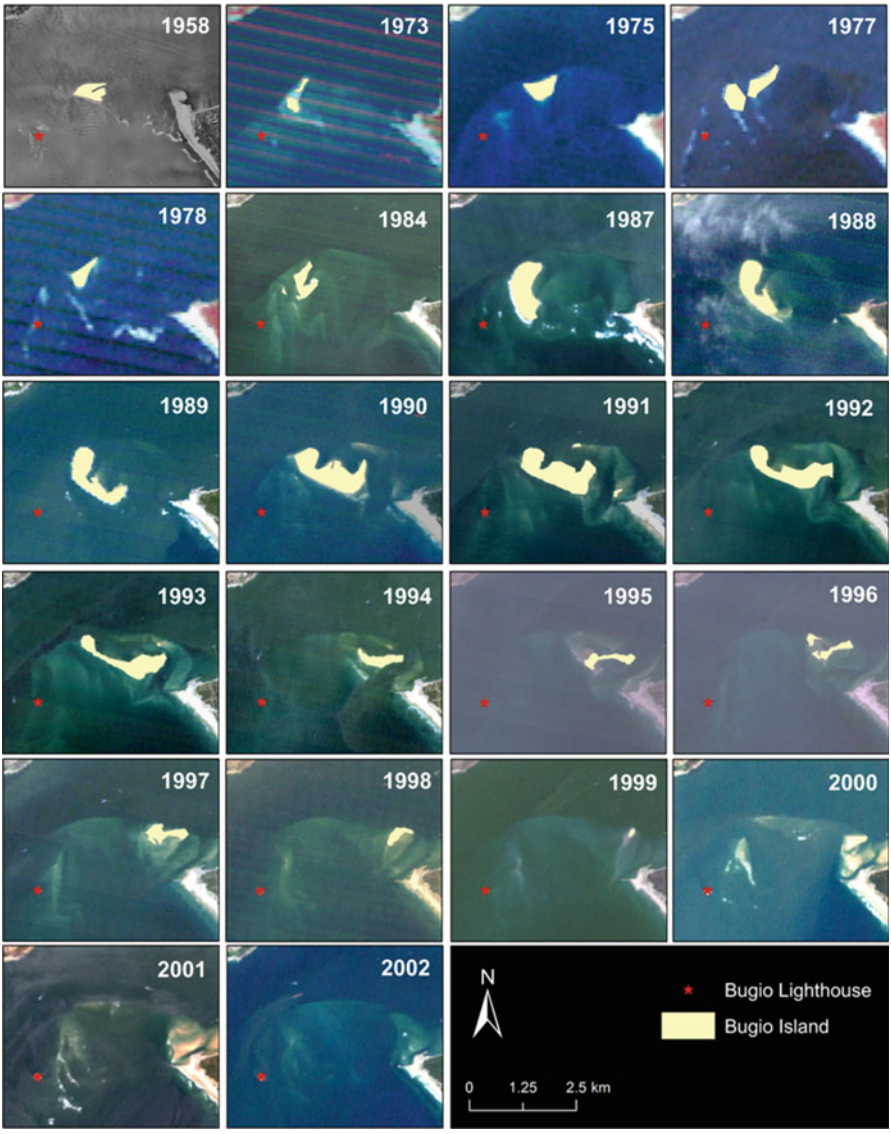

Fig. 4.5 Evolution of the Bugio Island between the years 1958 and 2002. Base map images: 1958 – aerial photograph; 1973–1978 – Landsat MSS 754 false color images, 1984–1999 – Landsat TM true color images; 2000–2002 – Landsat ETM + true color images

4.5.3.2 Results

The short-term evolution of Prainha beach is displayed on Fig. 4.7. The comparison of the shoreline extracted from satellite with field data showed a reasonable match, validating the applied methodology.

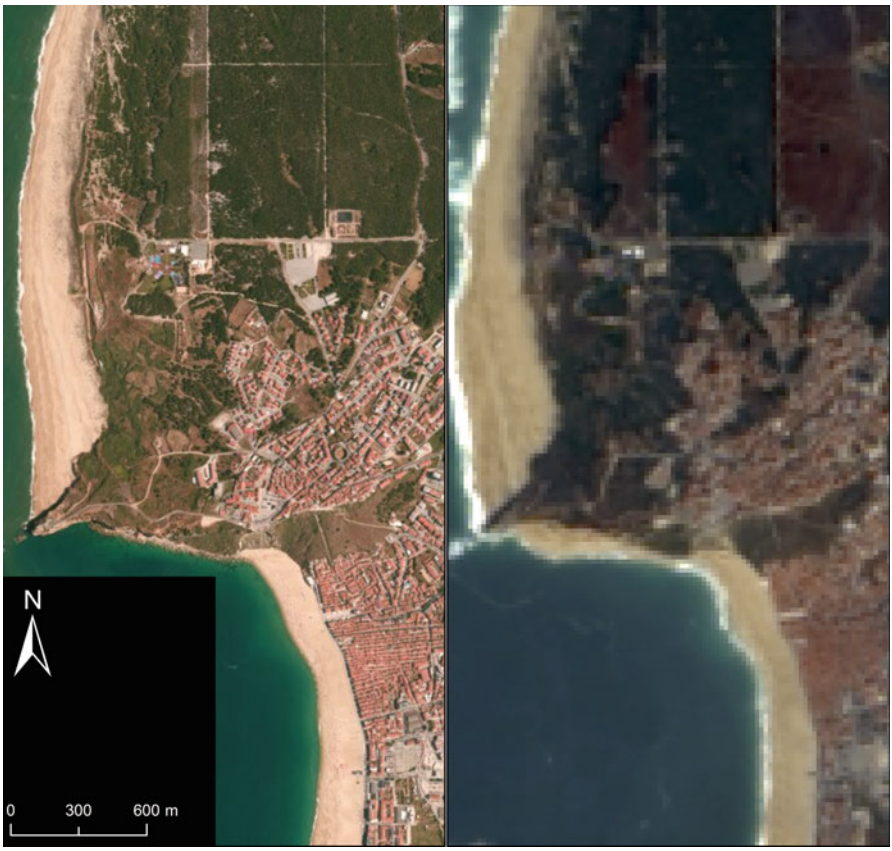

Fig. 4.6 Ephemeral beach development. *Left*: no ephemeral beach south of the Nazaré headland (Source: Esri basemap, 2011-03-18). *Right*: beach development south of the Nazaré headland visible on the Landsat 8 image of 2013-09-24

The beach started to develop on July, 2013 and has reached its maximum extent by the end of September, with ~1 km in length and ~100 m width. After that, and until mid October, the beach migrated eastwards with a noticeble retreat on the western section while preserving more less the area and shape. By the end of October, the beach receded and became significantly shorter, with a maximum width of ~50 m. From this point onwards the beach fades-out progressively until it will eventually vanishes (Fig. 4.6 – right).

The 16 days Landsat frequency of coverage appears to be effective in the attempt to study and monitor these type of seasonal phenomena, allowing the mapping of shoreline evolution and configuration, effectively complementing fieldwork experiments and data.

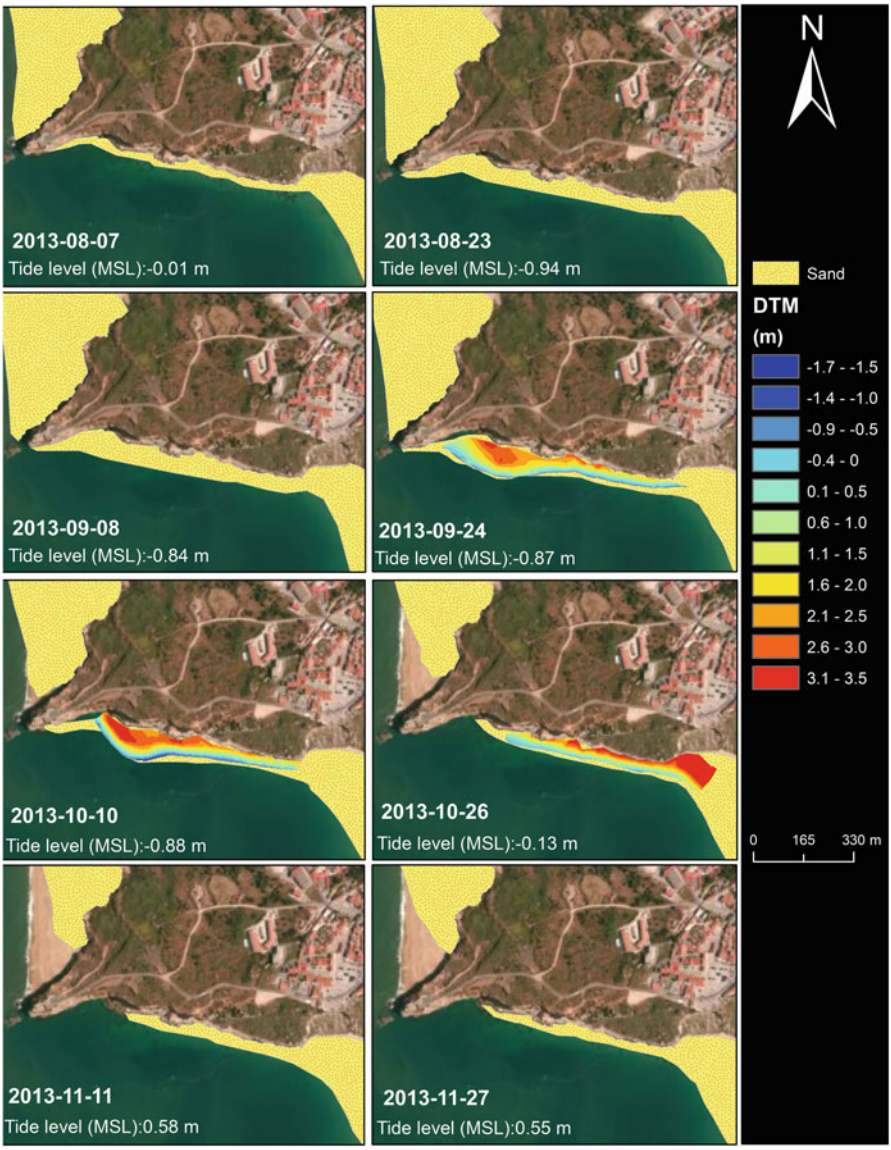

Fig. 4.7 Evolution of the ephemeral beach south of the Nazaré headland. The sand feature extracted by satellite imagery and DTM is the field validation

4.5.4 Bathymetric Data Retrieval

Airborne hyperspectral sensors are the best ones to derive bathymetric data, reducing the problem of spectral coverage, but they are still inappropriate for monitoring dynamical processes (Durand et al. 2000). Although passive optical systems are

limited in water depth penetration and constrained by water turbidity (Stumpf and Holderied 2003), the use of this type of data might be the only viable way to characterize extensive shallow-water areas, extremely dynamic regions or areas not covered by other, more accurate, methods.

The Landsat 8 coastal aerosol band (Band 1: 0.4333–0.4530 μm) has two objectives: (1) estimate the concentration of aerosols in the atmosphere, which may be used to refine the atmospheric correction procedures such as dark object subtraction and (2) provide new studies of the coastal and inland waters. Relative to the MODIS and the SeaWiFS sensors, the Landsat 8 allows for better imaging of these shallow water areas due to its superior spatial and radiometric resolutions (Table 4.1).

The following application example intends to demonstrate the potential of this new spectral band to derive and map shallow-water bathymetry.

4.5.4.1 Methodology

The bathymetry was derived using the bottom albedo[2]-independent bathymetry algorithm developed by Stumpf and Holderied (2003). This algorithm is based on the hypothesis that when the sea floor is covered by bright sand, the albedo is the same when the bottom is at the same depth. When the water is clear, this algorithm is capable of extracting the bathymetry up 25 m water depths; however results are intended to offer a general overview of the bathymetry and to highlighted relative changes and should not be used for navigational purposes. The pre-processing stage should include sun de-glinting (Hochberg et al. 2003; Hedley et al. 2005), because water usually presents variable sun glint across images, as a result of the ocean swell, causing widely variable incident angles for the reflection of the Sun's radiation, which may mask bottom features. Additionally, water should be as clear as possible, so that turbidity doesn't mask bottom albedo.

In this work, the bathymetry of Sado river ebb-delta (Fig. 4.1d) was derived from two Landsat images (Table 4.5) using the R-G-B-NIR bands. The difference in both images was the representation of the blue radiation range: Landsat 7 image used the ETM + Band 1 while the Landsat 8 image used the OLI Band 1 (coastal aerosol band).

4.5.4.2 Results

The shallow water bathymetry over the outer section of the Sado estuary derived from the Landsat imagery can be observed in Figs. 4.9 and 4.10. Results obtained from both images exhibits an overall pattern that closely matches the information portrayed in the nautical chart (Fig. 4.8). In fact, all the major morphological features, as the main channel, the ebb-tide delta and the Campanário tidal flats

[2] Albedo – the proportion of the incident light or radiation that is reflected by a surface.

Table 4.5 Landsat images used to derive bathymetry, date, time and respective tide level

Landsat sensor	Date	Time (UTC)	Tide (MSL) (m)
ETM+	2008-10-20	11:03:16	−0.60
OLI	2013-09-08	11:16:32	−0.84

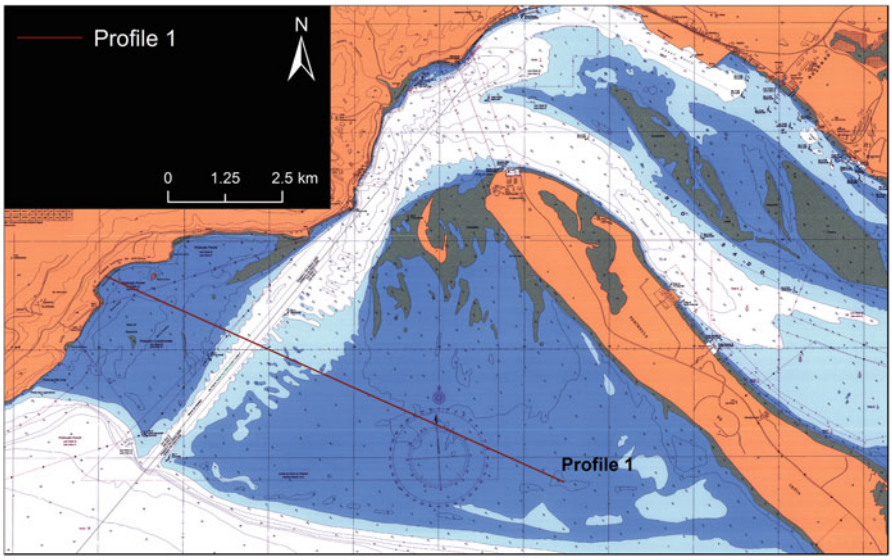

Fig. 4.8 Nautical Chart (November 2008) and localization of profile 1

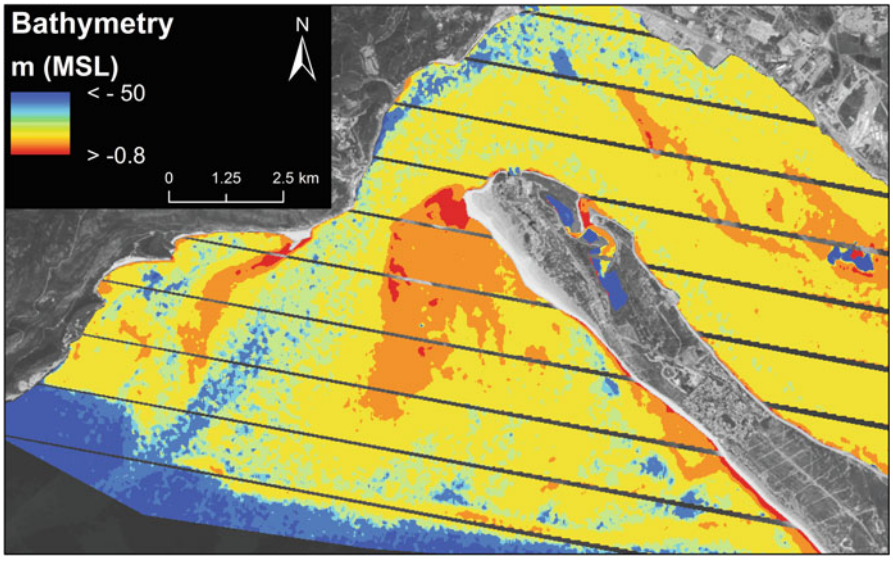

Fig. 4.9 Bathymetric derived data from 2008-10-20 Landsat 7 image

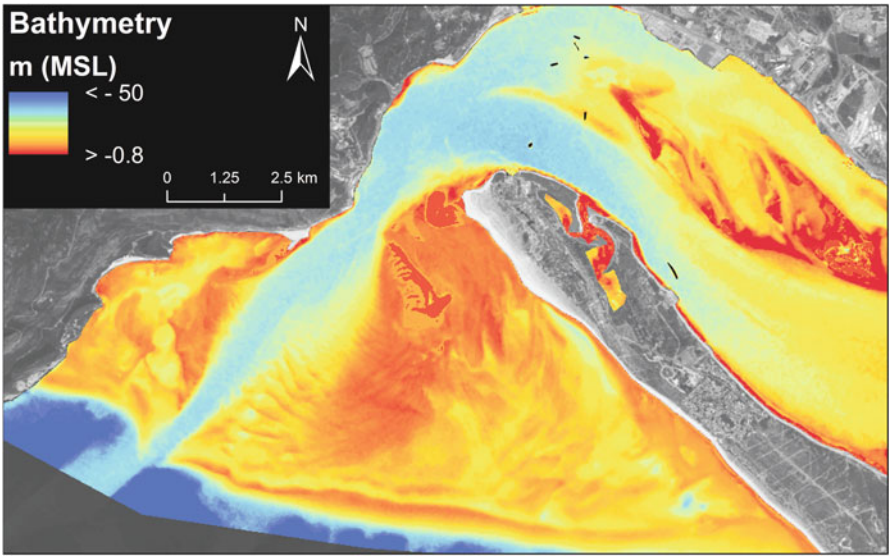

Fig. 4.10 Bathymetric derived data from 2013-09-08 Landsat 8 image

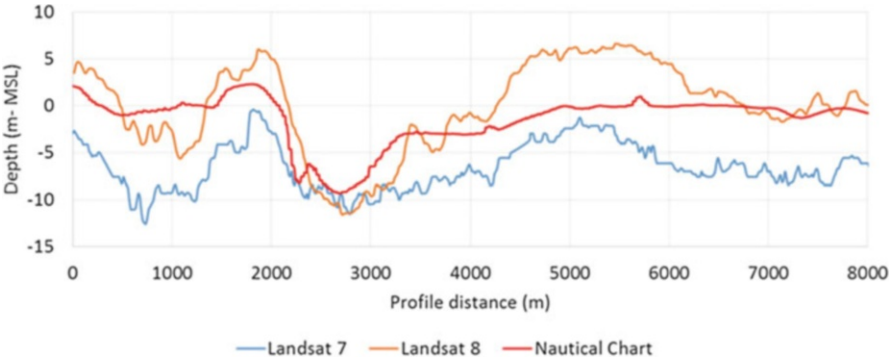

Fig. 4.11 Bathymetry derived from Landsat 7 (2008-10-20) and Landsat 8 (2013-09-08) in comparison with the nautical chart

display a very similar configuration. When comparing Landsat 7 with the Landsat 8 derived bathymetry, is possible to see that the former is clearly noisier, while Landsat 8 enables an impressive representation of the bathymetry over the area, with a detail that makes possible the definition of the bedform geometry over the entire ebb delta.

The larger bathymetric differences between images are observed over the Cambalhão shoal since this is area subject to significant morphological changes over time; to a large extent these discrepancies can be justified by the differences in the date of acquisition. A test profile (Profile 1 – Fig. 4.8) over the ebb delta that cross the main channel was performed in the three data sources. Results (Fig. 4.11)

show a reasonable agreement between satellites derived data and the bathymetric chart, which is better for the Landsat 8 image. The weak resolution of the bathymetric chart precludes a more detailed comparison but is sufficient to demonstrate the huge potentiality of the Landsat 8 images to derive bathymetric data.

4.6 Conclusion

This work synthetizes the application of satellite imagery to the study of mesoscale coastal processes. From the available sensors, the Landsat program stands out as the tool that offers the best compromise between potential and availability to the understanding of coastal dynamics at time scales spanning from months to decades and spatial scales from hundreds of meters to tens of kilometers. The 16 days Landsat frequency of coverage appears to be effective in the attempt to study and monitor seasonal phenomena such as beach rotation and sediment bypassing, while the temporal coverage (40 years) of this program allows the characterization of decadal shoreline changes. The recent launch of Landsat 8, with improved spectral and radiometric resolutions, further enhances its capabilities in what concerns shoreline detection and shallow water bathymetry extraction.

Acknowledgments Landsat images from the years 1991 to 1998 are data provided by the European Space Agency, in the frame of ESA Project – ID 14512 – An Integrated Approach to Shoreline Evolution: Application to West Portuguese Coast. The remaining Landsat images are available at the USGS website (http://earthexplorer.usgs.gov/).

The first author is supported by a Postdoc grant funded by the Fundação para a Ciência e Tecnologia – FCT (grant # SFRH/BPD/81800/2011). The authors are also supported by the Beach to Canyon project – Beach to Canyon Head Sedimentary Processes (# PTDC/MAR/114674/2009).

The authors would also like to thanks Ana Bastos for the vectorization of the nautical chart and Mónica Ribeira for the review.

References

Ahmad SR, Lakhan VC (2012) GIS-based analysis and modeling of coastline advance and retreat along the coast of Guyana. Mar Geod 35:1–15. doi:10.1080/01490419.2011.637851

Alesheikh A, Ghorbanali A, Nouri N (2007) Coastline change detection using remote sensing. Int J Environ Sci Technol 4:61–66

Boak EH, Turner IL (2005) Shoreline definition and detection: a review. J Coast Res 14:688–703

Durand D, Bijaoui J, Cauneau F (2000) Optical remote sensing of shallow-water environmental parameters: a feasibility study. Remote Sens Environ 73(2):152–161. doi:10.1016/S0034-4257(00)00090-0

Ford M (2013) Shoreline changes interpreted from multi-temporal aerial photographs and high resolution satellite images: Wotje Atoll, Marshall Islands. Remote Sens Environ 135:130–140. doi:10.1016/j.rse.2013.03.027

Gens R (2010) Remote sensing of coastlines: detection, extraction and monitoring. Int J Remote Sens 31:1819–1836. doi:10.1080/01431160902926673

Goward SN, Williams DL (1997) Landsat and earth systems science: development of terrestrial monitoring. Photogramm Eng Remote Sens 63(7):887–900

Hedley JD, Harborne AR, Mumby PJ (2005) Simple and robust removal of sun glint for mapping shallow-water benthos. Int J Remote Sens 26(10):2107–2112. doi:10.1080/01431160500034086

Hochberg EJ, Andrefouet S, Tyler MR (2003) Sea surface correction of high spatial resolution Ikonos images to improve bottom mapping in near-shore environments. IEEE Trans Geosci Rem Sens 41(7):1724–1729

Horn DP (2002) Mesoscale beach processes. Prog Phys Geogr 26:271–289. doi:10.1191/0309133302pp336pr

Huang H, Liu Y, Qiu Z (2012) Morphodynamic evolution of the Xiaoqing River mouth: a Huanghe River-derived mixed energy estuary. Chin J Oceanol Limnol 30:889–904. doi:10.1007/s00343-012-1295-4%201

Ikeda M, Dobson FW (1995) Oceanographic applications of remote sensing. CRC Press, New York

Klemas V (2001) Remote sensing of landscape-level coastal environmental indicators. Environ Manage 27:47–57. doi:10.1007/s002670010133

Klemas V (2009) Sensors and techniques for observing coastal ecosystems. In: Yang X (ed) Remote sensing and geospatial technologies for coastal ecosystem assessment and management, Lecture notes in geoinformation and cartography. Springer, Berlin/Heidelberg, 561 p. doi:10.1007/978-3-540-88183-4 1

Klemas V (2011) Remote sensing techniques for studying coastal ecosystems: an overview. J Coast Res 27:2–17. doi:10.2112/JCOASTRES-D-10-00103.1

Martin S (2004) An introduction to remote sensing. Cambridge University Press, Cambridge

Mather PM (2004) Computer processing of remotely-sensed images: an introduction. Wiley, Chichester

Mika AM (1997) Three decades of Landsat instruments. Photogramm Eng Remote Sens 63(7):839–852

Morton RA, Speed FM (1998) Evaluation of shorelines and legal boundaries controlled by water levels on sandy beaches. J Coast Res 14:1373–1384

Mukhopadhyay A (2012) Automatic shoreline detection and future prediction: a case study on Puri Coast, Bay of Bengal, India. Eur J Remote Sens 45:201–213. doi:10.5721/EuJRS20124519

NASA. Landsat 7 science data user's handbook. Available online: http://ltpwww.gsfc.nasa.gov/IAS/handbook/handbook_toc.html

NOAA. Coastal change analysis program regional land cover. Available online: http://www.csc.noaa.gov/digitalcoast/data/ccapregional

Parker BB (2003) The difficulties in measuring a consistently defined shoreline – the problem of vertical referencing. J Coast Res Spec Issue 38:44–56

Pe'eri S, Azuike C, Alexander L, Parrish C, Armstrong A (2012) Beyond the chart: the use of satellite remote sensing for assessing chart adequacy and completeness information. In: Proceedings of the 2012 Canadian hydrographic conference: the Arctic, old challenges, new approaches, Niagara Falls, Canada, 15–17 May

Ryu JH, Kim CH, Lee YK, Won JS, Chun SS, Lee S (2008) Detecting the intertidal morphologic change using satellite data. Estuar Coast Shelf Sci 78:623–632. doi:10.1016/j.ecss.2008.01.020

Short NM, Lowan PD, Freden SC, Finch WA (1976) Mission to earth: Landsat views the world, NASA special publication 360. NASA Science and Technical Information Office, Washington, DC

Stumpf RP, Holderied K (2003) Determination of water depth with high-resolution satellite imagery over variable bottom types. Limnol Oceanogr 48(1):547–556

Thieler ER, Himmelstoss EA, Zichichi JL, Ergul A (2009) The Digital Shoreline Analysis System (DSAS) version 4.0: an ArcGIS extension for calculating shoreline change. U.S. Geological Survey, Reston. Open Report 2008–1278

USGS. Landsat Mission Timeline. Available online: http://landsat.usgs.gov/about_mission_history.php

Williamson RA (1997) The Landsat legacy: remote sensing policy and the development of commercial remote sensing. Photogramm Eng Remote Sens 63(7):877–885

Yang X (2009) Remote sensing, geospatial technologies and coastal ecosystems. In: Yang X (ed) Remote sensing and geospatial technologies for coastal ecosystem assessment and management. Lecture notes in geoinformation and cartography. Springer, Berlin/Heidelberg, p 561. doi:10.1007/978-3-540-88183-4%201

Yu K, Hu C, Muller-Karger F (2011) Shoreline changes in west-central Florida between 1987 and 2008 from Landsat observations. Int J Remote Sens 32(23):8299–8313. doi:10.1080/01431161.2010.535045